

**PROCESSING, MICROSTRUCTURE AND PROPERTIES OF IN SITU  
COPPER REINFORCED TUNGSTEN CARBIDE  
NANOSTRUCTURED COMPOSITE**

**by**

**MAHANI BINTI YUSOFF**

**Thesis submitted in fulfillment of the  
requirements for the degree  
of Doctor Philosophy**

**Mei 2012**

## **ACKNOWLEDGEMENTS**

Since the beginning of my study, I have been accompanied and supported by many people. It is a pleasant opportunity for me to express my gratitude for all of them in this thesis.

I am deeply indebted to my supervisor, Assoc. Prof. Dr. Zuhailawati Hussain who kept an eye on the progress of my work and always was available when I needed her advises. Thank you for patiently responding to my enquiries and reinforcing my views. I am also very grateful to my co-supervisor, Prof. Radzali Othman.

I take this opportunity to express my deep sense of gratitude to the Dean, Prof. Ahmad Fauzi Mohd Noor and all staffs of School of Materials and Mineral Resources Engineering, Universiti Sains Malaysia (USM). I would like to say a very special ‘thank you’ to Mr. Kemuridan for guiding in using the planetary ball mill machine. To Mr. Shahrul, who help very much on the successful of sintering processes; to Mr. Zaini, Mr. Rashid, Mr. Khairi for their help in SEM and XRD analysis.

My gratitude extends to Ministry of Science, Technology and Innovation (MOSTI) for National Science Fellowship and USM for RU-PRGS grant.

I would like to record my thanks to all my fellow colleagues (Nur Hawadah, Mohd Salihin, and Long) for providing a stimulating and fun learning environment.

Last but by no means least; I wish to thank my family for their encouragement and ongoing support during the whole process of my education. To my beloved mother, a million thank to you. You raised me, supported me, taught me, and loved me; to her I dedicate this thesis.

## TABLE OF CONTENTS

	<b>Page</b>
<b>ACKNOWLEDGEMENTS</b>	ii
<b>TABLE OF CONTENTS</b>	iii
<b>LIST OF FIGURES</b>	viii
<b>LIST OF TABLES</b>	xvi
<b>LIST OF SYMBOLS</b>	xvii
<b>LIST OF ABBREVIATIONS</b>	xx
<b>LIST OF PUBLICATIONS</b>	xxii
<b>ABSTRAK</b>	xxiii
<b>ABSTRACT</b>	xxv

## **CHAPTER 1 – INTRODUCTION**

1.1 Introduction	1
1.2 Problem statement	4
1.3 Research objectives	5
1.4 Research scope	5

## **CHAPTER 2 – LITERATURE REVIEW**

2.1 Introduction	7
2.2 Metal matrix composite	7
2.2.1 Copper-based composite	8

2.2.2 Tungsten carbide as a reinforcement phase	11
2.2.3 Copper-tungsten carbide composite	16
2.3 Powder metallurgy of copper-based composite	18
2.3.1 Conventional mixing	20
2.3.2 Compaction	21
2.3.3 Sintering	23
2.3.4 Advancement in powder metallurgy route	25
2.4 In situ processing	26
2.5 Mechanical alloying (MA)	27
2.5.1 General characteristics and mechanism	27
2.5.2 Milling time	32
2.5.3 Milling speed	34
2.5.4 Ball to powder ratio	37
2.5.5 Process control agent	38
2.5.6 Ball size	40
2.6 Nanostructured materials prepared by mechanical alloying	42
2.7 Mechanical alloying of binary Cu- $x$ system	43
2.8 Characterizations of mechanical alloying product	44
2.8.1 X-ray diffraction	45
2.8.2 Crystallite size and internal strain	47
2.8.3 X-ray photoelectron spectroscopy	51
2.9 Summary	57

## **CHAPTER 3 – MATERIALS AND METHODOLOGY**

3.1 Introduction	59
3.2 Preparation of composite powder	59
3.2.1 Raw materials	59
3.2.2 Composite composition	61
3.2.3 Preparation of unmilled Cu-W-C powder mixture	62
3.3.4 Mechanical alloying	62
3.3 Preparation of bulk composite	64
3.3.1 Compaction	65
3.3.2 Sintering	65
3.4 Phase and microstructure observations	66
3.4.1 X-ray diffraction	66
3.4.2 Rietveld analysis	66
3.4.3 Crystallite size and internal strain	67
3.4.4 Lattice parameter	68
3.4.5 X-ray photoelectron microscopy	69
3.4.6 Scanning electron microscopy	70
3.4.7 Laser diffraction particle size	71
3.5 Properties characterizations	71
3.5.1 Green and sintered density	71
3.5.2 Hardness measurement	72
3.5.3 Electrical conductivity measurement	73

## **CHAPTER 4 – RESULTS AND DISCUSSION**

4.1 Introduction	74
4.2 Raw material characterization	74
4.3 Effect of milling time	76
4.3.1 XRD pattern of as-milled powder	76
4.3.2 Crystallite size and internal strain of as-milled powder	81
4.3.3 Lattice parameter of as-milled powder	85
4.3.4 SEM images of as-milled powder	87
4.3.5 Particle size distribution	91
4.3.6 XRD patterns of sintered compact	92
4.3.7 Tungsten carbide phase quantification	98
4.3.8 Crystallite size of sintered compact	99
4.3.9 XPS analysis of sintered compact	100
4.3.10 SEM images of sintered compact	105
4.3.11 Properties of sintered compact	108
4.4 Effect of milling speed	113
4.4.1 XRD patterns of as-milled powder	113
4.4.2 Crystallite size and internal strain of as-milled powder	115
4.4.3 Lattice parameter of as-milled powder	118
4.4.4 SEM images of as-milled powder	119
4.4.5 Particle size distribution	121
4.4.6 XRD patterns of sintered compact	123
4.4.7 Tungsten carbide phase quantification	125

4.4.8 SEM images of sintered compact	126
4.4.9 Properties of sintered compact	128
4.5 Effect of compaction pressure	131
4.5.1 SEM images of sintered compact	131
4.5.2 Properties of sintered compact	133
4.6 Effect of sintering temperature and time	138
4.6.1 XRD pattern characteristics of sintered compact	139
4.6.2 Tungsten carbide phase quantification	141
4.6.3 SEM images of sintered compact	143
4.6.4 Properties of sintered compact	144

## **CHAPTER 5 – CONCLUSIONS**

5.1 Conclusions	148
5.2 Suggestions for future work	150

## **REFERENCES**

## **APPENDICES**

Appendix A Derivations

Appendix B Calculations

## LIST OF FIGURES

Fig. 2.1	Tungsten carbide phase diagram	15
Fig. 2.2	Microstructure of sintered Cu-WC composite	18
Fig. 2.3	Rearrangement of particles during powder compaction	22
Fig. 2.4	The mechanism of particles coalescence during sintering a) initial contact (b) necking and growth (c) neck growth and (d) fully coalesced	24
Fig. 2.5	Powder entrapments during ball to ball collision in MA	28
Fig. 2.6	Three stages in mechanically alloyed Al-4.5wt.%Cu at (a) 4 h (early stage) (b) 8 h (intermediate stage) and (c) 10 h (final stage)	30
Fig. 2.7	SEM images of (a) initial Cu powder (b) initial pure W powder and (c) W-Cu powder mixture milled for 4 h, Cu (grey area) and tungsten (white area)	31
Fig. 2.8	The effect of milling time on Fe contamination level in mechanically alloyed W-C powder	33
Fig. 2.9	Rotation of the ball and powder corresponding to the motion of container in planetary ball mill	35
Fig. 2.10	The effect of weight of the balls on Fe crystallite size	41
Fig. 2.11	Plot of $B_{\parallel} \cos\theta$ against $\sin\theta$ , indicating the intercept and the slope used to calculate the crystallite size and internal strain	50
Fig. 2.12	XPS photoelectron emission process	53

Fig. 2.13	Curve fitting with spectrum deconvolution and Shirley background of (a) Cu 2p <sub>3/2</sub> for pure Cu powder and (b) Nb 3d for Cu-NbC composite at various milling time	55
Fig. 2.14	XPS spectra of doublets W 4f (W 4f <sub>7/2</sub> and W 4f <sub>5/2</sub> ) and C 1s with increasing carburization time	56
Fig. 3.1	Experimental process flow for in situ copper-tungsten carbide composite preparation and characterization	60
Fig. 3.2	Example of sintering profile for 900°C with heating and cooling rate of 5°C/min with 1 h soaking time	65
Fig. 4.1	XRD patterns of elemental (a) Cu powder (ICSD-98-005-7417) (b) Cu sintered pellet (ICSD-98-005-7417) (c) W powder (ICSD-98-009-1529) and (d) graphite powder (ICSD: 98-005-2931)	75
Fig. 4.2	Density distribution of Cu, W and graphite powders	76
Fig. 4.3	XRD pattern of unmilled powder mixture	77
Fig. 4.4	XRD patterns of as-milled powder after milled at (a) 10 h (b) 20 h (c) 40 h and (d) 60 h for the powder milled with 10 mm ball	78
Fig. 4.5	XRD patterns of as-milled powder after milled at (a) 10 h (b) 20 h (c) 40 h and (d) 60 h for the powder milled with 20 mm ball	80

Fig. 4.6	Plot of $B_r \cos\theta$ against $\sin\theta$ for calculating crystallite size and internal strain for the powder milled with (a) 10 mm ball and (b) 20 mm ball	82
Fig. 4.7	Cu crystallite size and internal strain of as-milled powder with different milling times	83
Fig. 4.8	Dislocation density of as-milled powder with different milling times	84
Fig. 4.9	Cu lattice parameter of as-milled powder with different milling times	86
Fig. 4.10	(a) SEM images of unmilled powder and corresponding EDX analysis on (b) X1 area and (d) Y1 area	87
Fig. 4.11	SEM images of as-milled powder milled at (a) 10 h (b) 20 h (c) 40 h and (d) 60 h for 10 mm ball with corresponding EDX analysis for (e) X2 area and (f) Y2 area	89
Fig. 4.12	SEM images of as-milled powder milled at (a) 10 h (b) 20 h (c) 40 h and (d) 60 h for 20 mm ball with corresponding EDX analysis for (e) X3 area and (f) Y3 area	90
Fig. 4.13	$d(4,3)$ of as-milled powder with different milling times	91
Fig. 4.14	Density distribution of as-milled powder with different milling times	92
Fig. 4.15	XRD pattern of sintered unmilled compact prepared by sintering at 900°C	93

Fig. 4.16	XRD patterns of sintered compact milled at (a) 10 h (b) 20 h (c) 40 h and (d) 60 h and sintered at 900°C for the powder milled with 10 mm ball	94
Fig. 4.17	XRD patterns of sintered compact milled at (a) 10 h (b) 20 h (c) 40 h and (d) 60 h and sintered at 900°C for the powder milled with 20 mm ball	97
Fig. 4.18	W <sub>2</sub> C and WC relative weight percent (wt.%) with different milling times and sintered at 900°C	99
Fig. 4.19	Cu crystallite size of sintered compact with different milling times	100
Fig. 4.20	XPS wide scan for (a) unmilled sintered compact (b) sintered compact milled at 40 h for 10 mm ball	101
Fig. 4.21	XPS curve fitting for (a) Cu 2p (b) C 1s and (c) W 4f of unmilled sintered compact prepared by sintering at 900°C	102
Fig. 4.22	XPS curve fitting for (a) Cu 2p (b) C 1s and (c) W 4f of sintered compact prepared by milling at 40 h and sintering at 900°C	104
Fig. 4.23	SEM image of unmilled sintered compact prepared by sintering at 900°C	105
Fig. 4.24	SEM images of sintered compact milled at (a) 10 h (b) 20 h (c) 40 h and (d) and sintered at 900°C for the powder milled with 10 mm ball	106

Fig. 4.25	(a) SEM image and elemental mapping on the corresponding area of (b) all elements (c) Cu (red) (d) W (green) (e) Fe (indigo) and (f) C (yellow) in sintered compact milled at 40 h and sintered at 900°C for 10 mm ball	107
Fig. 4.26	SEM images of sintered compact milled at (a) 10 h (b) 20 h (c) 40 h and (d) 60 h and sintered at 900°C for the powder milled with 20 mm ball	108
Fig. 4.27	Green density (GD) and sintered density (SD) of powder compact with different milling times	109
Fig. 4.28	Hardness of sintered compact with different milling times	111
Fig. 4.29	Electrical conductivity of sintered compact with different milling times	112
Fig. 4.30	XRD patterns of as-milled powder after milling for (a) 100 rpm (b) 200 rpm and (c) 300 rpm for the powder milled with 10 mm ball and 40 h	114
Fig. 4.31	XRD patterns of as-milled powder after milling for (a) 100 rpm (b) 200 rpm and (c) 300 rpm for the powder milled with 20 mm ball and 40 h	115
Fig. 4.32	Cu crystallite size and internal strain of as-milled powder with different milling speeds	117
Fig. 4.33	Dislocation density of as-milled powder with different milling speeds	118

Fig. 4.34	Cu lattice parameter of as-milled powder with different milling speeds	119
Fig. 4.35	SEM images of as-milled compact milled at (a) and (b) 100 rpm (c) and (d) 200 rpm and (e) and (f) for 300 rpm and sintered at 900°C, for the powder milled with 10 mm and 20 mm ball, respectively	120
Fig. 4.36	$d_{(4,3)}$ of as-milled powder with different milling speeds	122
Fig. 4.37	Density distribution of as-milled powder with different milling speeds	123
Fig. 4.38	XRD patterns of sintered compact milled at (a) 100 rpm (b) 200 rpm and (c) 300 rpm and sintered at 900°C for the powder milled with 10 mm ball	124
Fig. 4.39	XRD patterns of sintered compact milled at (a) 100 rpm (b) 200 rpm and (c) 300 rpm and sintered at 900°C for the powder milled with 20 mm ball	125
Fig. 4.40	$W_2C$ and WC weight percent (wt. %) with different milling speeds sintered at 900°C	126
Fig. 4.41	SEM images of sintered compact milled at (a) and (b) 100 rpm (c) and (d) 200 rpm and (e) and (f) for 300 rpm and sintered at 900°C, for the powder milled with 10 mm and 20 mm ball, respectively	127
Fig. 4.42	Green density (GD) and sintered density (SD) of powder compact with different milling speeds	129

Fig. 4.43	Hardness of sintered compact with different milling speeds	130
Fig. 4.44	Electrical conductivity of sintered compact with different milling speeds	131
Fig. 4.45	SEM images of as-milled powder compacted at (a) 100 MPa (b) 400 MPa and (c) 600 MPa and sintered at 900°C for the powder milled with 10 mm ball	133
Fig. 4.46	Green density (GD) and sintered density (SD) of sintered compact with different compaction pressures	135
Fig. 4.47	Plot of experimental data for green compact using the equation proposed by Panelli and Ambrozio Filho (1998)	136
Fig. 4.48	Hardness of sintered compact with different compaction pressures	137
Fig. 4.49	Electrical conductivity of sintered compact with different compaction pressures	138
Fig. 4.50	XRD patterns of sintered compact milled at 40 h and sintered at (a) 800°C, 1 h (b) 900°C, 1 h (c) 1000°C, 1 h (d) 900°C, 2 h and (e) 900°C, 3 h for the powder milled with 10 mm ball	140
Fig. 4.51	XRD patterns of sintered compact milled at 40 h and sintered at (a) 800°C, 1 h (b) 900°C, 1 h (c) 1000°C, 1 h (d) 900°C, 2 h and (e) 900°C, 3 h for the powder milled with 20 mm ball	141

Fig. 4.52	WC relative weight fraction (wt.%) of sintered compact with different sintering temperatures	142
Fig. 4.53	SEM images of sintered compact milled and sintered at (a) 850°C and (b) 1050°C for the powder milled with 10 mm ball (b) and (c) 850°C and (d) 1050°C for the powder milled with (c) 20 mm ball	144
Fig. 4.54	Density of sintered compact with different compaction pressures	145
Fig. 4.55	Hardness of sintered compact with different sintering temperatures	146
Fig. 4.56	Electrical conductivity of sintered composite with different sintering temperatures	147

## **LIST OF TABLES**

Table 2.1	Properties of various copper based composites prepared by powder metallurgy	11
Table 2.2	Several techniques found in literatures that have been used to synthesize copper-based composite for various ceramic reinforcement	19
Table 3.1:	Several properties of Cu, W and graphite cited from Habashi, Callister, Lassner and ASM International Handbook	61
Table 3.2	Detailed milling parameter for composite preparation	63
Table 3.3	Characterization of milling speed according to $r_c$ and $\Omega$ (rpm)/ $\omega$ (rpm)	64

## LIST OF SYMBOLS

<b>Symbol</b>	<b>Description</b>
$\langle D \rangle$	Crystallite size
$\Delta\rho_{gb}$	Resistivity due to grain boundary
$A$	Parameter due to plastic deformation
$a, c$	Lattice parameter
$a_0$	True lattice parameter
$A_c$ and $D_c$	Constant (using Cohen's method)
$B$	Full width at half maximum
$B$	Parameter represents apparent density
$B_0$	Sum of total broadening
$B_{crystallite}$	Broadening due to size
$B_i$	Broadening due to instrumental
$B_r$	Overall broadening after subtraction of instrument broadening
$B_{strain}$	Broadening due to strain
$D$	Diffusion coefficient
$d$	Spacing between two adjacent planes
$d$	Arithmetic mean
$D$	Relative density
$D_0$	Diffusion constant
$E_b$	Binding energy

$E_k$	Kinetic energy
$F$	Applied load
$h$	Planck's constant
$H_V$	Vickers hardness
$k$	Constant
$l_c$	Distance from rotation shaft to centroid of a ball
$m$	Ball mass
$m_a$	Mass in the air (using Archimedes's principle)
$m_w$	Mass in water(using Archimedes's principle)
$n$	Integral number of adjacent plane
$N$	Dislocation density
$Q$	Activation energy
$R$	Boltzman's constant
$r$	Vial radius
$r_b$	Ball radius
$r_c$	Critical speed ratio
$R_{dv}$	Distance between disc center and vial center
$R_{exp}$	Expected error
$R_p$	Profile residual
$R_r$	Revolution radius
$R_{wp}$	Weight-pattern profile
$S$	Goodness of fit
$S_r$	Grain boundary surface area

$T$	Temperature
$TD_{comp}$	Theoretical density of composite
$TD_{Cu}$	Theoretical density of Cu
$TD_{WC}$	Theoretical density of tungsten carbide
$\nu$	Frequency of the excitation radiation
$V$	Volume
$V_c$	Collision velocity
$y_b(i)$	Background intensity
$y_c(i)$	Calculated intensity at point $i$
$\eta$	Internal strain
$\theta$	Angle of scattering
$\lambda$	Radiation wavelength
$\rho$	Conductivity
$P_{Me\_gb}$	Spesific grain resistivity
$\rho_w$	Water density
$\sigma$	Resistivity
$\varphi$	Work function of spectroscopy
$\Omega$	Disc rotation speed
$\omega$	Vial rotation speed

## LIST OF ABBREVIATIONS

<b>Abbreviation</b>	<b>Description</b>
BSE	Back scattered electron
DEM	Discrete element model
EDX	Energy dispersive X-ray
ESCA	Electron spectroscopy for chemical analysis
FAT	Fixed analyzer transmission
FESEM	Field emission scanning electron microscopy
FWHM	Full width at half maximum
GD	Green density
GOF	Goodness of fit
IACS	International annealed copper standard
ICDD	International center for diffraction data
ICSD	Inorganic crystal structure database
MA	Mechanical alloying
MMC	Metal matrix composite
ODS	Oxide dispersion strengthened
PBTC	2-phosphono-butane-1, 2, 4-tricarboxylic acid
PCA	Process control agent
PM	Powder metallurgy
RIR	Relative intensity ratio
RSF	Relative sensitivity factor

SD	Sintered density
SE	Secondary electron
SEM	Scanning electron microscopy
TD	Theoretical density
TEM	Transmission electron microscopy
UHV	Ultra high vacuum
UTS	Ultimate tensile strength
WA	Warren-Averbach method
WH	Williamson-Hall method
XPS	X-ray photoelectron spectroscopy
XRD	X-ray diffraction

## LIST OF PUBLICATIONS

1. **Mahani Y.**, Radzali O., Zuhailawati H., Mechanical alloying and sintering of nanostructured tungsten carbide-reinforced copper composite and its characterization. **Materials and Design** 2011; 32: 3293-3298.
2. Zuhailawati H., Salihin H.M., **Mahani Y.**, Microstructure and properties of copper composite containing in situ NbC reinforcement: Effects of milling speed. **Journal of Alloys and Compounds** 2010; 489: 369-374.
3. Zuhailawati H and **Mahani Y.**, Effects of milling time on hardness and electrical conductivity of in situ Cu-NbC composite produced by mechanical alloying. **Journal of Alloys and Compounds** 2009; 476: 142-146.
4. Zuhailawati H., **Mahani Y.**, Radzali O., Phase analysis of mechanically alloyed in situ copper-tungsten carbide composite. **Advanced Materials Research** 2011;173:67-71.
5. Zuhailawati H. and **Mahani Y.**, **Fabrication and characterization of in-situ synthesis of niobium carbide reinforced iron composite by mechanical alloying**, accepted to be published in chapter in book for Metal Matrix Composite.
6. **Mahani Y.** and Zuhailawati H., **Effect of milling condition on the microstructure and the properties of nanostructured copper tungsten carbide composite**. The International Conference for Nanomaterials Synthesis and Characterization (INSC 2011), Seri Kembangan, Selangor, 4-5 July 2011. Poster presentation.
7. **Mahani Y.**, Radzali O., Hussain Z., **Microstructure investigations of in-situ copper tungsten composite by mechanical alloying**, International Conference on X-rays and Related Technique in Research and Industry 2010, Langkawi, Kedah, 9-10 June 2010. Oral presentation.
8. Zuhailawati H., Othman R., **Mahani Y.**, Umemoto M. **Effect of milling time on phase and properties of in-situ copper base composite prepared by mechanical alloying technique**. Conference and Exhibition of Composite Materials and Nanostructures (IC2MS'08), Melaka, 5-7 August 2008.
9. Zuhailawati H. and Mahani Y., **In-situ formation of NbC mechanically alloyed Cu-Nb-C at different temperature**, International Conference on Mechanochemistry and Mechanical Alloying (INCOME2008), Jamshedpur, India, 1–4 December, 2008.

# **PEMPROSESAN, MIKROSTRUKTUR DAN SIFAT-SIFAT KOMPOSIT IN SITU KUPRUM DIPERKUAT TUNGSTEN KARBIDA BERSTRUKTUR NANO**

## **ABSTRAK**

Kajian ini bertujuan untuk menyiasat ciri-ciri dan sifat-sifat in situ komposit kuprum tungsten karbida berstruktur nano yang dihasilkan oleh pengaloian mekanikal dan metallurgi serbuk. Serbuk kuprum (Cu), tungsten (W) dan grafit (C) dikisar di dalam pengisar bebola planetari mengikut saiz bola, masa dan kelajuan pengisaran berbeza. Kemudian, serbuk tersebut dimampat pada tekanan berbeza dan disinter pada suhu dan masa berlainan. Pembentukan tungsten karbida secara in situ berlaku selepas pengaloian mekanikal dan pensinteran.  $W_2C$  terbentuk terlebih dahulu dan pembentukan WC berlaku pada masa dan kelajuan pengisaran yang dilanjutkan, yang disertai dengan pengurangan saiz hablur dan peningkatan terikan dalaman semasa pengaloian mekanikal.  $W_2C$  terbentuk disebabkan oleh kekurangan C, manakala WC terbentuk melalui penjelmaan daripada  $W_2C$  kepada WC semasa pensinteran. Sifat kekerasan meningkat manakala kekonduktiviti elektrik menurun dengan peningkatan masa (10 hingga 40 jam) dan kelajuan pengisaran (100 hingga 400 rpm). Peningkatan tekanan pemampatan membawa kepada penumpatan komposit dan ini menyebabkan kekerasan dan kekonduktiviti elektrik juga meningkat. Walaubagaimanapun, kekerasan tidak dapat ditingkatkan walaupun suhu pensinteran ditingkatkan yang mana ianya berpuncu dari peningkatan keliangan di dalam komposit. Untuk peningkatan masa pengisaran, bola 20 mm tidak dapat menyebabkan penghasilan saiz hablur yang halus dan terikan dalaman lebih besar berbanding saiz bola 10 mm. Akibatnya, WC terbentuk pada masa pengisaran lebih pendek bagi bola 10 mm berbanding bola 20 mm. Disebabkan oleh tenaga hentaman lebih besar diperoleh dari taburan pelanggaran (dengan bola bersaiz 10 mm) berbanding daya hentaman (dengan bola bersaiz 20 mm), bola 10 mm menunjukkan sifat-sifat kekerasan dan kekonduksian elektrik

lebih baik. Walau bagaimanapun, peningkatan kelajuan pengisaran (100 kepada 300 rpm), komposit menggunakan bola 20 mm dilihat mempunyai sifat-sifat lebih baik berbanding komposit dihasilkan menggunakan bola 10 mm. Untuk pembolehubah tekanan pemampatan dan suhu pensinteran, sifat kekerasan dan kekonduksian elektrik lebih tinggi untuk komposit yang dikisar menggunakan bola 10 mm berbanding bola 20 mm. Kekonduksian elektrik untuk komposit berasaskan kuprum yang tinggi dihasilkan melalui pengisaran pada 40 jam dan 400 rpm dengan bola 10 mm bersama-sama dengan pemampatan pada 300 MPa dan suhu pensinteran pada 900°C.

# **PROCESSING, MICROSTRUCTURE AND PROPERTIES OF IN SITU COPPER REINFORCED TUNGSTEN CARBIDE NANOSTRUCTURED COMPOSITE**

## **ABSTRACT**

The present work investigates characteristics and properties of in situ nanostructured copper-tungsten carbide composite prepared by mechanical alloying (MA) and powder metallurgy (PM). Elemental powders of Cu (copper), W (tungsten) and graphite (C) were milled in a planetary ball mill using different ball size, milling time and milling speed. Then the product was compacted at different pressures and sintered at different temperatures and times. In situ tungsten carbide phases (WC and W<sub>2</sub>C) were only present after a combination of MA and sintering. W<sub>2</sub>C was first to be observed and the formation of WC began with longer milling times and speeds, in accordance to a decreased crystallite size and an increased of internal strain of Cu during MA. W<sub>2</sub>C was formed as a result of C deficiency whereas WC through transformation from W<sub>2</sub>C to WC during sintering. Hardness of composite was enhanced but electrical conductivity was reduced with increasing milling time and milling speed. Higher applied pressure leads to higher densification of composite where hardness and electrical conductivity was also improved. However, the hardness was not improved even though densification has been enhanced with increasing sintering temperature which was resulted from the increased of porosity within the composites. Upon increasing milling time, ball size with 20 mm did not lead to smaller crystallite size and larger internal strain compared to that of 10 mm. Consequently, in situ WC was formed earlier with 10 mm ball than with 20 mm ball size. Due to greater impact energy that has been produced by collision frequency (with 10 mm ball size) rather than impact force (with 20 mm ball size) at increasing milling time, the result of hardness and electrical conductivity was shown better for 10 mm ball. However, the increase of milling speed (100 to 300 rpm) with 20 mm ball size was observed to have better properties than 10 mm

ball. Upon increased of compaction pressure and sintering temperature both hardness and electrical conductivity is higher for 10 mm ball compared to that of 20 mm. High conductivity copper-based composite was produced through milling at 40 h and 400 rpm with 10 mm ball associated with compaction at 300 MPa and sintering temperature at 900°C.

# **CHAPTER 1**

## **INTRODUCTION**

### **1.1 Introduction**

Copper (Cu) generally is known as a base metal having high electrical conductivity and good corrosion and oxidation resistance but low in strength. Its limitation is being improved by purposely dispersing a hard ceramic phase into it. There has been much attention in recent years focusing on copper-based composite reinforced with transition metal carbides, borides and nitrides. Among these phases, carbides and oxides are frequently used as reinforcement materials that are homogenously dispersed in Cu matrix. The advantage is they can retard particle coarsening during annealing, in order to retain the strength of the composite. Tungsten carbide is a refractory metal with a high melting point (2777°C) (Cardarelli, 2008), high hardness (1000 kg/mm<sup>2</sup>) at elevated temperatures (López *et al.*, 2007), excellent resistance to oxidation and a high thermal stability. These unique properties make tungsten carbide suitable for the reinforcement of soft Cu to improve of Cu's mechanical properties.

Copper-based composite benefits from its excellent electrical properties, thermal conductivity and good resistance to oxidation and are mostly utilized in electrical application (Lee and Kim, 2004). One of the most significant electrical applications of copper-tungsten carbide composite is as a material for electrical contact which is widely used in high voltage switches, circuit breakers, relays and welding electrodes (Minakova *et al.*, 1983). Electrical contact material must be chosen on the basis of high electrical conductivity, strength, resistance to wear and a high melting point (Grill *et al.*, 2005).

Copper-tungsten carbide composite is a potential candidate to replace Ag based electrical contact since it has an almost similar electrical conductivity and an excellent resistance to arc compared to Ag based alloys, but also can be produced at a lower cost. A reinforced phase plays an important role in the enhancement of mechanical and electrical conductivity properties of Cu-based composite (Rajkovic *et al.*, 2008a). The reinforced phase can be used incorporated into metal matrix (ex situ processing) or synthesized within the metal matrix (in situ processing).

Recently, copper-tungsten carbide composite electrical contact has been fabricated mostly by powder metallurgy (PM) through powder blending, compacting and sintering. More advanced methods, for example, PM coupled with mechanical alloying (MA) imparts a large amount of interest among several researchers. High energy milling can promote MA, a process that causes severe mechanical plastic deformation of the entrapped powders due to ball-to-ball and ball-to-wall collisions, significantly enhancing the generation of dislocation. At the beginning of MA, cold welding is a dominant event and with a prolonged milling process, fracturing and rewelding would take place. Powder fracturing during MA introduces defects into the powder and generates new clean surfaces that are beneficial for atomic diffusion. As microstructural refinement progresses, a steady state deformation is reached when a balance between fractures and cold welding has been attained. The MA technique combined with in situ processing has been developed to synthesize reinforcement directly in the metal matrix during metal matrix composite (MMC) fabrication via chemical reaction between the raw materials (Tjong and Ma, 2000). A MMC fabricated through in situ processing has finer powder particles and exhibits outstanding mechanical properties that are achieved only with

difficulty through conventional ex situ processing. It is known that nanostructured material produces a great deal of superior mechanical properties. MA is generally able to produce nanostructured materials (Koch, 2007; Wu and Li, 2000). Heavily deformed microstructure as a result of MA consists of a wide variety of defects such as dislocation, stacking faults and twin boundaries that are able to reduce grain size into nano-scale. In the method of combination of MA and PM, the MA mechanism is used to promote the diffusion process by producing nanostructure while sintering is expected to enhance the diffusion by forming a new phase. This approach has been employed for many systems such as Fe-Al-Ti-C (Krasnowski and Kulik, 2008), Cu-TiB<sub>2</sub> (Dong *et al.*, 2002), Fe-TiC (Wang and Wang, 2007) and Al-Cu-C (Reyes *et al.*, 2009). Therefore, it is possible to fabricate nanostructured copper-tungsten carbide composite which combines the high conductivity of Cu and the excellent mechanical and physical properties of its extremely fine grained nanocrystalline structure by MA and PM which can be a candidate to be used in high performance electrical applications.

Synthesizing in situ copper-tungsten carbide composite was previously conducted by Baikalova *et al.* (2000). They have proved that it was possible to form in situ tungsten carbide in Cu matrix by PM and MA. Microstructure and properties of mechanically alloyed materials are very sensitive to MA conditions. Several parameters that have been studied by a number of researchers on mechanically alloyed copper-based composite including milling time, speed, ball to powder ratio, ball size, temperature and type of atmosphere. Duration of milling has a remarkable influence on phase and microstructure evolution during solid state reactions in mechanically alloyed powder as well as on the properties of the sintered product (Hewitt and Kibble, 2009).

## **1.2 Problem statement**

Most studies on the fabrication of copper-tungsten carbide composite synthesis use a particle dispersion method for the strengthening mechanism. Even though they used a combination method of MA and PM, the discussion is only limited on using commercial tungsten carbide as a reinforced phase. Preliminary work on milling of elemental Cu, W and graphite mixture was undertaken by Baikalova *et al.* (2000), who successfully fabricated copper-tungsten carbide composites with various compositions of mixture Cu, W and C powders in a short milling time. Although they showed that the dispersion of tungsten carbide in Cu matrix by MA through in situ processing is possible, further information on this technique still remains unavailable in the literature. Besides, the authors did not offer clear explanations on microstructural and structural evolutions such as in situ tungsten carbide phase formation ( $W_2C$  and WC), dissolution activity, structural refinement as well as corresponding composite properties. Two tungsten carbide phases (WC and  $W_2C$ ) are generally observed upon heat treatment of in situ consolidated copper-tungsten carbide composite. In the study of MA of elemental W and C powders, Bolokang *et al.* (2010) mentioned that the degree of formation for these two tungsten carbide phases mainly influenced by a variation of milling parameters. Hence, it is of great interest to study microstructure and properties of the composite by explaining it through the governing parameters of MA and PM.

Microstructure and properties of mechanically alloyed materials are very much dependent on MA conditions. All the studies reviewed so far, however, do not consistently explain the effects of impact energy and frequency on the as-milled powder and sintered product. Also, a much comprehensive discussion on the correlation of

milling time and milling speed with microstructural and structural properties for nanostructured in situ copper-tungsten carbide composite has not yet been discussed in literatures. To some extent, the effect of compaction and sintering parameters on the properties of sintered copper-tungsten carbide composite should also be explained.

### **1.3 Research objectives**

The main interest in this work was to develop a technique combining MA and PM for the incorporation of tungsten carbide particles into a Cu matrix, taking advantage of the chemical reaction between W and graphite powders that is promoted by MA, resulting in in situ nanostructured copper-tungsten carbide. Therefore, the objectives of this research are:

- i. To understand in situ formation of tungsten carbide in sintered Cu-W-C milled mixture prepared by MA and PM.
- ii. To investigate the influence of milling (in terms of milling time, milling speed and ball size) and consolidation parameters (consist of compaction pressure and sintering temperature and time) on the microstructure and properties of in situ copper-tungsten carbide composites.
- iii. To evaluate the relationship between MA and PM parameters in fabrication of in situ nanostructured copper-tungsten carbide composite.

### **1.4 Research scope**

In this research, in situ copper-tungsten carbide composite with corresponding composition of Cu-30vol.%WC was prepared by MA and PM using elemental Cu, W

and graphite powders. Evolution of in situ composite microstructure and properties was classified and explained in terms of milling, compaction and sintering parameters. For MA, milling durations of 10, 20, 40 and 60 h and milling speed of 100, 200, 300 and 400 rpm were used as studied parameters. Dependencies of the above variables were also considered for instance, when milling time was selected as the desired parameters; 400 rpm (with maximum speed for Frisch Pulvirestte 5) was used as a fixed milling speed. MA parameters are initiated for large internal refinement for diffusion in order to produce nanostructured composites. In order to elucidate the effect of impact energy during MA, two ball sizes were used for the experiments.

Cold compaction was used to produce bulk composite and the pressure was varied from 100 to 600 MPa, in order to observe the effects of the consolidation process on composites. The composite green body which was compacted at 300 MPa was reproduced for a set of milling and sintering parameters. Sintering at different temperatures and times were performed to investigate in situ reinforced phase formation in Cu matrix and its corresponding properties. For all sets of milling parameters and compaction pressure, the green compact was sintered at 900°C. Sintered composites were characterized by means of density, hardness and electrical conductivity. Changes in hardness and electrical conductivity due to phase formation and microstructure alteration were evaluated according to milling, compaction and sintering parameters. Improved properties of milled in situ copper-tungsten carbide composite were compared with unmilled Cu-W-C mixtures which were compacted and sintered in a similar process as preparing the mechanically alloyed Cu-W-C mixture.

## CHAPTER 2

### LITERATURE REVIEW

#### **2.1 Introduction**

This chapter seeks to accommodate the theory within which the research was undertaken. It is intended to describe the metal matrix composite (MMC) of copper-based composites and its reinforcement phase of tungsten carbide. A detail description on powder metallurgy (PM), mechanical alloying (MA) and the in situ method used to produce the copper-tungsten carbide composite is also focused in this chapter. Finally, the end of this chapter describes the common analysis method for microstructural and the structural properties of MA and PM products.

#### **2.2 Metal matrix composite**

The constituent materials that often do not possess very good properties on their own, when combined, produce some very attractive materials. In composite materials, when the matrix is a metal or alloy, it can be classed as MMC. Most MMCs were developed to increase the strength of conventional metals. However, properties of MMC which are determined mainly by reinforcement chosen for enhancing yields and tensile strength and/or to improve corrosion, wear and thermal shock resistance. MMCs have long been developed and used in aerospace and automotive applications. For instance, titanium-based composite was a very common material used in high stressed wings area in a part wings-fuselage joint.

Although MMC has not been commercially produced as much as metal alloys, it is recognized as the most promising candidate for high temperature applications with high

strength. Metal can be strengthened in many ways such as by solid solution hardening, grain size reduction, and dislocation strengthening. Solid solution hardening involves adding atoms of the reinforced phase into the lattice of matrix, resulting in either a substitution or an interstitial solid solution while dislocation strengthening and grain size reduction is in respect of the plastic deformation from applied stress. This study is based on tungsten carbide reinforced copper composite, therefore Cu based composite and tungsten carbide will have their elaboration in the following section.

### **2.2.1 Copper-based composite**

There is considerable interest in MMC for various matrix of based metal such as Cu, magnesium (Mg), titanium (Ti), cobalt (Co) and nickel (Ni) (Chawla and Chawla, 2006). Among these, Cu possesses excellent resistance towards corrosion and oxidation. It is more favorable among other common metals in electrical applications because of its excellent electrical and thermal conductivity (Wu *et al.*, 2005). Even though Cu resistivity ( $1.7 \mu\Omega\text{cm}$ ) is not much different from that of silver resistivity ( $1.6 \mu\Omega\text{cm}$ ) (Venugopal *et al.*, 2007), Cu has been used as the common material for high temperature conductor (700 to  $800^\circ\text{C}$ ). Despite its excellence in electrical conductivity, Cu suffers low specific strength at higher temperatures which limits its application especially when there is a combination of both electrical and mechanical strength required. The need for materials with such demands are desirable mostly in applications including sliding electrical contacts and collectors (Yilmaz and Aksoy, 2001), resistance welding electrodes (Venugopal *et al.*, 2007), heat exchangers and rocket nozzles (Groza and Gibeling, 1993).

PM parts made by Cu-W or Cu-graphite alloy are usually used as materials for high resistance against arcing or welding (Davis, 2001). It has been reported that electrical conductivity of Cu alloys could reach as high as 80% IACS with 600 MPa in tensile strength (Takahashi and Hashimoto, 1991). Two methods, either by age hardening or incorporating a hard phase into Cu matrix have been applied to improve the mechanical properties of Cu. Cu alloys produced by precipitation hardening imposed high ultimate tensile strength (UTS) up to 1000 MPa (Akhtar *et al.*, 2009). However, developing copper-based materials by incorporating second phase reinforcement is much preferable since it distinguishes a lack of solubility of precipitate second phase in Cu at lower temperatures by precipitation hardening. In addition, age hardened alloys often demonstrate lower strength at higher temperature (Botcharova *et al.*, 2004) due to the growth or dissolution of precipitate phase (Akhtar *et al.*, 2009) hence, needing an appropriate heat treatment. Incorporating hard phase into Cu by means of copper-based composite not only enhances the mechanical properties of Cu, but also retains its electrical and thermal performance. By embedding second phase into metallic matrix, the preparation of copper-based composite with materials having positive enthalpy of mixing becomes increasingly possible.

There has been much attention in recent years focusing on copper-based composite reinforced transition metal carbides, borides and nitrides. These ceramic reinforcements tend to show metal-like bonding with Cu. Also, they can retard particle coarsening during annealing in order to retain the strength of the composite. Reinforced particles in Cu matrix that have been commonly used are TiC (Akhtar *et al.*, 2009; Palma *et al.*, 2004; Rathod *et al.*, 2009), WC (Deshpande *et al.*, 2006; Deshpande and

Lin, 2006; Zhao *et al.*, 2004), NbC (Long *et al.*, 2010a; Long *et al.*, 2010b; Marques *et al.*, 2005; Takahashi and Hashimoto, 1991; Zuhailawati and Mahani, 2009; Zuhailawati *et al.*, 2010; Zuhailawati and Yong, 2009), TaC (Takahashi and Hashimoto, 1991), TiB<sub>2</sub> (Dong *et al.*, 2002; López *et al.*, 2005), SiC (Gan and Gu, 2008; Gan and Gu, 2006; Tjong and Lau, 2000b; Zhang *et al.*, 2008; Zurnachyan *et al.*), Al<sub>2</sub>O<sub>3</sub> (Kang, 2005a; Rajkovic *et al.*, 2010, 2008a; Rajkovic *et al.*, 2008b; Shehata *et al.*, 2009; Tian *et al.*, 2006; Upadhyaya and Upadhyaya, 1995) and ZrC (López *et al.*, 2007). Among these hard ceramic phases, carbides have been used extensively as a strengthener for Cu to increase both wear resistance and mechanical strength. In electro-friction applications for contact materials, carbide was purposely added to increase wear, arc and melting resistance (Yilmaz and Aksoy, 2001). Embedded carbide in Cu matrix acts to impede crack propagation during load transfers from matrix to reinforced phase with a condition that the modulus of reinforcement is higher than that of pure Cu (Yan and Geng, 2007).

In addition, introducing even a small amount of alloying or element of second phase to Cu will reduce its electrical conductivity. Table 2.1 shows the properties of various kinds of copper-based composites prepared by the PM method. The hardness, electrical conductivity and density values vary since the route and parameter in PM were different. It has been reported that the presence of fine TiB<sub>2</sub> within Cu matrix lowered the electrical conductivity of Cu-TiB<sub>2</sub> composite having 35.1% IACS than that of pure Cu (70.9% IACS) (López *et al.*, 2005). This composite was prepared by means of PM routes through high energy milling and sintering that uniformly distributed fine TiB<sub>2</sub> particle in Cu matrix. The presence of finely distributed TiB<sub>2</sub> particles within Cu matrix led to a change in hardness and electrical conductivity of Cu-TiB<sub>2</sub> composite.

Table 2.1: Properties of various copper-based composite prepared by powder metallurgy

Copper-based composite	Hardness (HV)	Electrical conductivity (% IACS)	Sintered density (g/cm <sup>3</sup> )	References
Cu-Y <sub>2</sub> O <sub>3</sub>	76	59	7.65	Stobrawa <i>et al.</i> , 2007
Cu-WC	70.3	55	7.706	Stobrawa and Rdzawski, 2009
Cu-NbC	23.4	18.2	5.81	Zuhailawati and Mahani, 2009
Cu-TiB <sub>2</sub>	160	35.1	-	López <i>et al.</i> , 2005
Cu-Al <sub>2</sub> O <sub>3</sub>	163.1	46	6.88	Rajkovic <i>et al.</i> , 2010

## 2.2.2 Tungsten carbide as a reinforcement phase

Tungsten carbide has unique properties such as a high melting point, extremely high hardness, fracture toughness, compressive strength and excellent corrosion resistance and thermal stability. In fact, tungsten carbide has low density (15.63 g/cm<sup>3</sup>) over W (19.3 g/cm<sup>3</sup>) (Deshpande and Lin, 2006). It has a high melting point (2777°C) (Cardarelli, 2008) and the hardest carbide at elevated temperatures (1000 kg/mm<sup>2</sup>) (Toth, 1971) and also retains its stability during heating and cooling (Deshpande and Lin, 2006). The most stable phase of tungsten carbide is WC which has a hexagonal structure with two atoms per unit *a* with *c/a* ratio of 0.976 (Swain, 1994). Synthesis of only WC single-carbide is practically impossible since there is semi carbide, W<sub>2</sub>C (Pierson, 1996).

Tungsten carbide has been synthesized by various methods of production. For example, heating the powder metal or W compounds with carbon or CH<sub>4</sub> (Storms, 1967) and by coating W with carbon (C) under argon flow by hydrocarbon gas followed by carburization and reduction of tungstic acid (Koc and Kodambaka, 2000; Zhang *et al.*, 2006). However, these two methods suffer from serious agglomeration and accumulate high cost of production attributed to high heating temperature. Direct carbothermic reduction of natural wolframite (FeWO<sub>4</sub>) by high energy ball milling was developed by Temuujin *et al.* (2005). Tungsten carbide has been observed as homogenously dispersed in the mixture which consists of FeWO<sub>4</sub> and active carbon. WC was formed through the conversion of intermediate carbide ternary phases, Fe<sub>6</sub>W<sub>6</sub>C and Fe<sub>3</sub>W<sub>3</sub>C after 2 h of milling and calcining at 1100°C. Passador *et al.* (2005) suggest that adding 5 wt. % KCl and 1 wt. % Ni during C reduction by wolframite may accelerate the formation of stable WC. Tungsten carbide can also be synthesized through the reduction reaction by tungsten oxide. Several researchers have successfully prepared tungsten carbide powders by reaction milling of WO<sub>3</sub>-Mg mixture (El-Eskandarany, 2000; Ma and Zhu, 2010; Tan *et al.*, 2000; Won *et al.*, 2008). The reduction of WO<sub>3</sub> by Mg was first induced by α-W formation through explosion in the vial. After that, the diffusion process took place with sufficient accumulation of heat during milling. According to Passador *et al.* (2005), the complete WC formation could be obtained by adding KCl and Ni during carburizing of WO<sub>3</sub>, without the intermediate phase of W<sub>2</sub>C. Synthesis of WC through ball milling of WO<sub>3</sub>-C-2Al has been studied by El-Eskandarany *et al.* (2005), Pallone *et al.* (2007) and Sakaki *et al.* (2009a; 2009b). They have all agreed that

the major phases in the final product either consist only of WC or the mixture of WC and W<sub>2</sub>C.

Most of the synthesis of tungsten carbide from elemental powders of W and C has been mostly carried out by ball milling. Wang *et al.* (1997) investigated the effect of milling time on WC structural evolution for 50:50 atomic structures of W and activated C powder. They have proposed that WC was produced by milling process not from heat treatment, by the comparison of their results at 45 h and 90 h of milling. However, heat treatment has been applied in order to comprise almost entirely of the crystalline structure from transition of W<sub>2</sub>C to WC at temperatures of 900°C. However, they only investigate the equal atomic mixture of W and C which then provide more available C in the system for WC formation. Another work by Bolokang *et al.* (2010) has shown that the higher C contents the longer the milling duration for a complete formation of WC. They have proposed that the success of producing a stable tungsten carbide is only determined at further milling time and at higher available C since the probability of W atoms to contact with C atoms is impeded by the initial formed WC. In contrast, W<sub>2</sub>C phase is determined at a carbon-deficient composition which has been induced at a lower milling time.

According to Tan *et al.* (2000), high energy ball milling may lead to a self propagating reaction. It can be explained by the enhancement of entropy (becomes more positive) at a certain extent by the milling event as a result of the grain refining process. Their experiment was based on the relationship between total energy transformation during milling with their estimation value of the energy and heat formation of the mixture WO<sub>3</sub> and graphite. During milling, the energy transferred to the powder is said

to be equal to that of the energy absorbed by the powder mixture which contributes to the total energy of formation. If the enthalpy change is higher than that of the energy formation, self propagating reaction may occur. Since the amount of total energy absorbed during collision satisfies this condition, the reaction is considered as self propagating and nanocrystalline  $\text{WC}_{1-x}$  phase is successfully produced.

In order to understand the formation of  $\text{W}_2\text{C}$  and  $\text{WC}$ , one can observe the tungsten carbide phase diagram. Fig. 2.1 shows the available phase diagram proposed by Okamoto (2008). W-C system consists of three phases of tungsten carbide;  $\text{WC}$ ,  $\text{W}_2\text{C}$  and  $\beta\text{-WC}_{1-x}$  which were found to be modified accordingly by temperature and concentration ranges.  $\text{WC}$  is also described as  $\alpha\text{-WC}$  which decomposes by melting congruently.  $\text{W}_2\text{C}$  is sub carbide having hexagonal structure with lattice parameter,  $a$  equal to 0.38 nm and  $c$  equal to 0.47 nm. While unstable  $\beta\text{-WC}_{1-x}$  is only formed even at higher temperature (above 1530°C), this phase diagram also accounts for the eutectoid decomposition of  $\text{W}_2\text{C}$  to  $\text{W}$  and  $\text{WC}$  that occurs at temperatures around 1300°C. It is obviously difficult to obtain only  $\text{WC}$  at lower temperatures because of inhomogeneous reaction in stoichiometric ratio between pure  $\text{W}$  and  $\text{C}$  during carburizing process. Upon cooling, instead of decarburization, the formation of  $\text{W}_2\text{C}$  and  $\text{WC}_{1-x}$  can occur because of metastability of W-C system (Demetriou *et al.*, 2002).

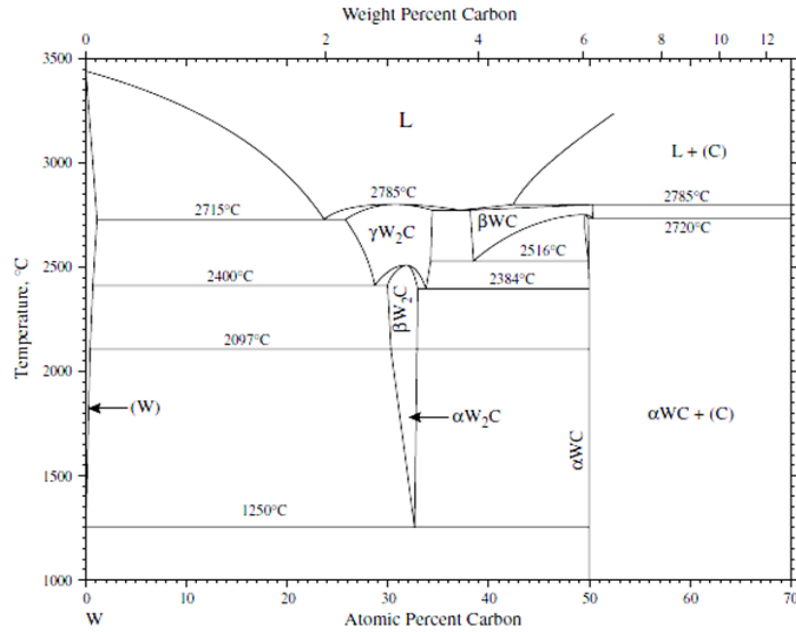
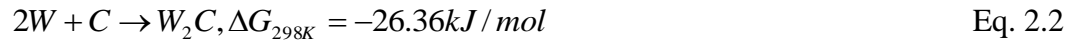


Fig. 2.1: Tungsten carbide phase diagram (Okamoto, 2008)

In terms of thermodynamic, a spontaneous reaction for tungsten carbide formation by milling has been proposed to occur according to the following equations (Yang *et al.*, 2011):



However, to obtain direct reaction of WC from Eq. 2.1, longer milling into several hundred hours might be required. Direct reaction of  $W + C \rightarrow WC$  was previously reported to have occurred at 1400 to 1600°C by Schwarzkopf and Kieffer (1953). Further, Gupta and Seigle (1975) observed that WC was stable at even lower temperature about 1300°C. Their experiment involves annealing the iron rod and the

mixture of W and WC under condition of the presence of oxygen. Upon heating, the interaction between oxygen and C from the powder mixture permits the calculation of carbon activity by the amount of accumulate C on the iron rods. With increasing temperature, C solubility is increased in tungsten and further precipitate WC phase.

WC and  $W_2C$  have nearly equal stabilities at room temperature since heat formation value of  $W_2C$  is only over 0.12 eV per C atom than WC (0.42 eV) (Cottrell, 1995). However,  $W_2C$  has been found to be unstable at lower temperatures ranging from 677 to 1000°C (Coltters and Belton, 1983). According to Kurlov and Gusev (2007), stability of  $W_2C$  depends on how much the randomize carbon atom is occupied along the site of its structure and it can be reached upon heat treatment at temperature above 1300°C. It can be observed by the proposed thermodynamic model of  $W_2C$  by Coltters and Belton (1983) using high temperature galvanic cell technique. They suggested that for the reaction of  $2W + C \rightarrow W_2C$ , the temperature for  $W_2C$  formation is in the range of 1300 to 2227°C.

### **2.2.3 Copper-tungsten carbide composite**

Good electrical conductivity from Cu matrix and high strength as well as excellent wear and corrosion resistance from tungsten carbide makes copper-tungsten carbide composite very useful in electrical with good wear resistance application. For instance, a potential candidate for contact material that used in welding electrodes. Copper-tungsten carbide composite has a very close electrical conductivity value (52% IACS) (Deshpande, 2006) with that of Ag based electrical contact (52.5% IACS) (Findik and

Uzun, 2003). Compared to the other reinforced phase, i.e. TiC and TiB<sub>2</sub>, WC has better wetting capabilities with Cu which lead to higher composite electrical conductivity.

Properties such as electrical conductivity, hardness and wear of copper-tungsten carbide composite have been widely studied by many researchers. Early work by Crysanthou *et al.* (1995) on synthesized copper-tungsten carbide composite is by injecting the ceramic reinforcement into Cu melts. Further, Deshpande *et al.* (2006) synthesized copper-tungsten carbide composite of composition Cu-53vol.%WC using infrared infiltration technique. They discovered that the electrical conductivity of composite is almost similar to that of commercially Cu-W composite. They suggested that the presence of carbide phase within the Cu matrix does not contribute to significant change in composite electrical conductivity since Cu network was continuously created surrounding the uniformly distributed WC particles. For a complete infiltrated composite, the hardness was also greatly increased when compared to the hardness of pure Cu.

Nowadays, copper-tungsten carbide composite has been mostly synthesized by PM route. This method will have its detailed discussion in the following section and here the discussion only restricted on the microstructure and properties of the copper-tungsten carbide composite prepared by PM. Fig. 2.2 shows the microstructure of PM-prepared copper-tungsten carbide composite by a work of Stobrawa and Rdzawski (2009). They have investigated mechanical and electrical properties of various amounts of commercial WC in Cu matrix. The microstructure consists of separated fine WC particles (white particles) embedded in Cu matrix (grey area). The composite sintered density (SD) is higher than that of sintered pure Cu while the hardness of Cu-

0.5vol.%WC composite is enhanced to 64.9 HV when it was compared with pure Cu (55 HV). Increasing volume fraction of WC leads to an increased of composite hardness. However, high electrical conductivity of Cu was sacrificed with increasing amount of WC fraction, two times below to that of sintered pure Cu.

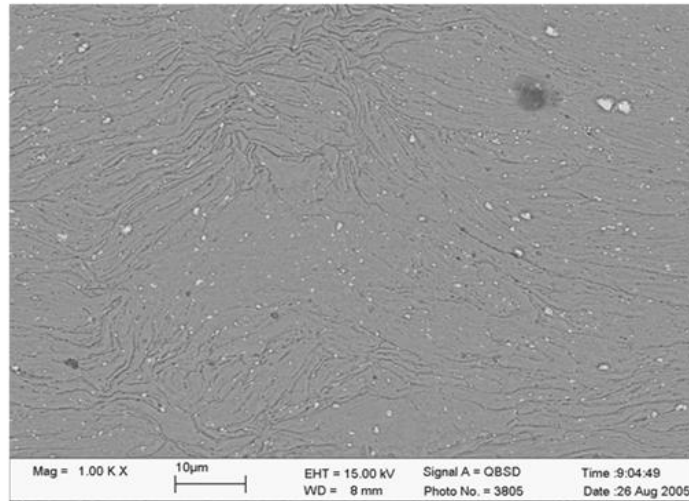


Fig. 2.2: Microstructure of sintered Cu-1.5wt. %WC composite (Stobrawa and Rdzawski, 2009)

### **2.3 Powder metallurgy of copper-based composite**

Table 2.2 shows common techniques that have been adopted to prepare copper-matrix composite reinforced hard ceramic. However, there are generally two methods that have been used to fabricate copper-based composite which are casting and melting and PM. Melting and casting is a liquid state processing which has been applied in most commercial application. The reasons are molten metal is cheaper and easier to handle than those of powders and also able to fabricate more varieties of shape and size of products. Over the years, copper-based composite has been synthesized by internal

oxidation method.  $\text{Al}_2\text{O}_3$  reinforced Cu is common composite produced by this method. The advantage is a very good distribution of fine oxide particles in Cu matrix which later may help to develop excellent mechanical properties of copper-based composite.

Table 2.2: Several techniques found in literatures that have been used to synthesize copper-based composite for various ceramic reinforcement

Copper-based composite	Method	References
Cu-TiC	MA, Self-propagation high temperature, Spray forming	Akhtar <i>et al.</i> , 2009, Chrysanthou and Erbaccio, 1996, Liang <i>et al.</i> , 2008, Palma <i>et al.</i> , 2004
Cu-WC	Pressureless infiltration, MA, Spray forming	Baikalova and Lomovsky, 2000, Deshpande <i>et al.</i> , 2006, Zuniga <i>et al.</i> , 2001
Cu-NbC	MA	Hussain <i>et al.</i> , 2008, Murphy and Courtney, 1994
Cu-TiB <sub>2</sub>	MA	Dong <i>et al.</i> , 2002, Ma and Tjong, 2000, Tu <i>et al.</i> , 2002
Cu-SiC	Pressureless infiltration, MA, Self-propagation high temperature	Shu and Tu, 2003, Zhang <i>et al.</i> , 2008, Zhu <i>et al.</i> , 2004
Cu-Al <sub>2</sub> O <sub>3</sub>	Pressureless infiltration, MA, Internal oxidation	Kang, 2005a, Lee and Kim, 2004, Thiraviam <i>et al.</i> , 2008,

For example, one of the studies of Rajkovic *et al.* (2008a) use low content of  $\text{Al}_2\text{O}_3$  to reinforce Cu matrix via internal oxidation. Cu-Al<sub>2</sub>O<sub>3</sub> mixture powders were milled in air in a planetary ball mill and hot pressed at 35 MPa. They revealed that hardness is around 1500 MPa in association with good electrical conductivity of 70% IACS. However, due to longer exposure time and restriction of contributing element to the oxidation make this method facing some disadvantages (Kaczmar *et al.*, 2000).

Immiscible systems such as Cu-W (Raghu *et al.*, 2001) and Cu-Ta (Mizutani and Lee, 1995; Venugopal *et al.*, 2007; Xu *et al.*, 1997) are difficult to be synthesized via casting or melting due to much difference in melting point of constituent element. Another drawback that has risen from liquid processing is poor distribution of ceramics reinforcements due to agglomeration and particle segregation.

All those restrictions by the methods can be minimized by dispersions strengthened of WC particles via PM. The ability to disperse very fine reinforced particles into Cu, leading to a better control of microstructure makes it the most promising method for Cu strengthening process. Before considering the uses of PM, one should take into account its mechanical behavior, chemical stability and thermal mismatch of selection of the materials. In general, PM route involves of blending or mixing, compaction, sintering and several finishing operations. Further explanation on procedure of conventional and advanced PM routes will be discussed in the next section.

### **2.3.1 Conventional mixing**

Mixing is such an important process in order to initiate distribution of powder particles as well as to minimize the porosity of the green body after consolidation as it is will affect final mechanical properties of the PM product. The main reason for mixing is to remove particle segregation. In general, segregation may be affected by particle shape, size and density. Irregular particle with fine particle size are to say inhibit particle segregation since the amount of interparticle friction is large. Mixing process only uses vibration transport to reduce segregation and thus it is commonly termed as conventional mixing. Conventional mixing does not change the original microstructure

of initial powder and solely distribute uniform reinforcement particles in the matrix. For industrial concern, conventional mixing is much preferred in economical ways but for scientific purposes more advanced methods are generally recommended.

### **2.3.2 Compaction**

Compaction is a process which involves converting the initial powders into dense and bulk materials in a die. The product of compacted powder is known as green compact. Densification can be done either under cold pressed or hot pressed, depending on the applications and the mechanical behavior desired. At first, the powder is cold pressed and if needed to increase the strength, the powders are mechanically pressed into a hot state. Hot pressed products normally consist of a very high relative density compared to cold pressed since both pressure and heat has been simultaneously applied.

Adherence of particles during compaction depends on powder shapes and sizes as well as powder distribution that have been introduced during mixing or blending. Two mechanisms are generally involved during compaction. At first, the particle exhibits sliding and rearrangement features where the particles are filling up the voids between them. Fig. 2.3 describes particle arrangement during compaction. The following stage where further compaction contributes to a better packing which increases the localized deformation, leading to porosity elimination (Davis and Committee, 2001). At this condition, particle size and shape may change due to fragmentation or elastic compression at particle contact points. With increasing compaction pressure, the rate of pores elimination will produce and there is a difference in shrinkage between areas to area. At this condition, the composite powder achieves early densification. Such

variation normally originates from the effect of condition of die wall friction, the internal friction between point contacts of particles, particle size distribution and sample size and shape. In fact, high SD is attributed by high homogeneities of density, packing and small particle size of green compact. Therefore, a great amount of initial point contact, small and uniform pores during compaction must contribute to shorter and lower sintering temperature and time.

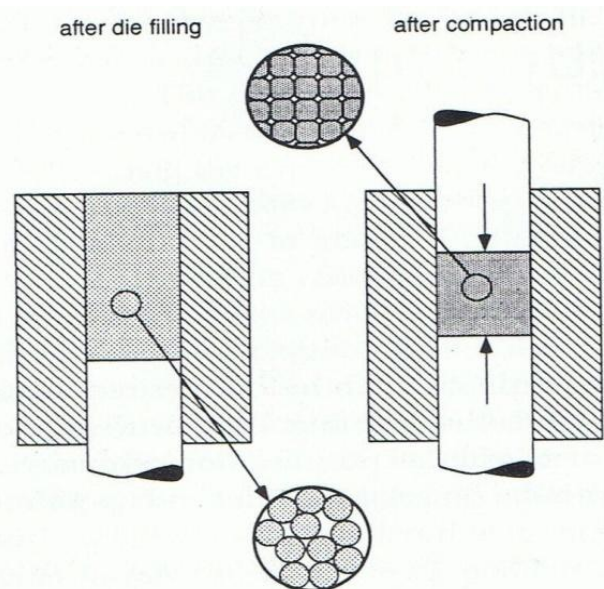


Fig. 2.3: Rearrangement of particles during powder compaction (Thummel and Oberacker, 1993)

The compressibility of powder mixture is affected by powder morphology and work hardening of hard particles within the composite. The spherical powder shape and smaller particle size is easier to be compact than the irregular powder and coarser particle size one. Higher work hardening may lower powder compressibility. It was shown that work hardening at high compaction pressure leads to reduce in

compressibility of Cu-SiC composite (Gan and Gu, 2008). It is also that too high applied pressure had increased the strength of Al-Al<sub>2</sub>O<sub>3</sub> composite as a result of work hardening. The reason because of the composite response for plastic deformation has been restricted (Hesabi *et al.*, 2007) by the presence of Al<sub>2</sub>O<sub>3</sub> particles.

### 2.3.3 Sintering

Sintering is a processing technique used to produce density-controlled materials by applying thermal energy (Kang, 2005b). In general, the sintering process can be divided into two types: solid state sintering and liquid state sintering. Solid state sintering occurs when the green compact is densified entirely in a solid state at particular sintering temperature. Meanwhile for liquid phase sintering, it occurs when a liquid phase is found in the green compact during sintering. The focus on this study is to sinter the powder compact in solid state; therefore the review on solid state sintering is only further explained.

Solid state sintering of green compact involves bonding together the particles by heating up to a temperature below the melting point of the major constituent element. Basic concept of solid state sintering can be illustrated by two intimate sphere creating a neck and grow to generate new grain boundary at the interface where the total interfacial energy reduce (Granger and Guizard, 2008). Fig. 2.4 shows the mechanism of two particles coalescence during sintering. After having sufficient time and energy, two particles are merged together into a single large particle. In short, two steps generally occur in sintering; grain growth and densification (German *et al.*, 1996). Surface and lattice diffusions are distinguished under grain growth since there is no densification

involves. Whereas grain boundary diffusion involves of filling the pores which increased the SD is under densification. This stage can be signified when residual porosity has been removed or shrinkage is occurring. In general, diffusion of atom occurs within microstructure when denser structure is obtained according to Eq. 2.3 (Callister, 2000):

$$D = D_0 \exp\left(\frac{-Q}{RT}\right) \quad \text{Eq. 2.3}$$

where  $D$  is the diffusion coefficient,  $D_0$  is constant,  $Q$  is the activation energy,  $R$  is Boltzman's constant and  $T$  is the temperature.

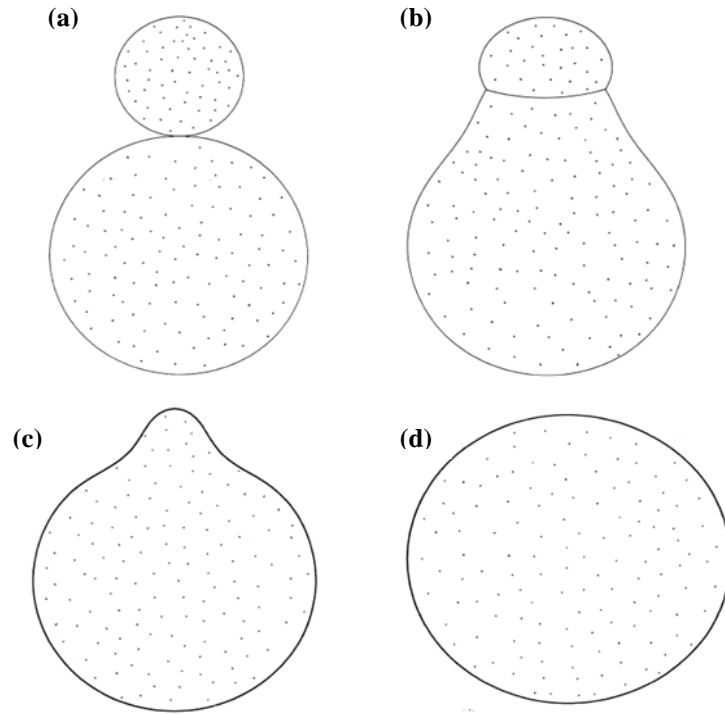


Fig 2.4: The mechanism of particles coalescence during sintering. (a) initial contact (b) necking and growth (c) neck growth and (d) fully coalesced (Pan *et al.*, 1998)

Many factors can be addressed to contribute for composite sintering abilities. They include green density (GD), constituent element, particle size, heating rate, sintering temperature, sintering time and sintering environment. Porosity could tremendously inhibit final properties of material if being neglected and has been found originates from many sources. When the level of pores is reduced, effective densification is usually obtained. In fact, the important key for elimination of pores is proper control of temperature, initial microstructure feature and heating cycle.

### **2.3.4 Advancement in powder metallurgy route**

PM through conventional processing often produces undesirable microstructure during densification as a result of poor sinterability which deteriorates final properties of the composite. Due to better dispersion of reinforcement by non-conventional PM, it is possible to incorporate hard ceramic phase in Cu. For instance, Gan and Gu (2008) have shown that PM via high energy milling produced homogenous distribution of SiC in Cu-SiC powder mixture. A recently developed method combining both PM and MA introduces excellent result on particle dispersion strengthening. Dong *et al.* (2002) coupled MA and hot pressing to explain the behavior of microstructure of in situ Cu-TiB<sub>2</sub>. They have proved that Ti and B are completely dissolved in Cu as well as formation of a very fine TiCu<sub>4</sub> phase to react with B to form TiB<sub>2</sub>.

Many techniques have been developed in order to combine both compaction and sintering in order to achieve high densified material for example, hot pressing (HP), hot isostatic pressing (HIP), spark plasma sintering (SPS) and resistance sintering. Tjong and Lau (2000a) examined the behavior of wear properties of Cu-TiB<sub>2</sub> produced by HIP